Classical and extended electrodynamics

Article *in* Physics Essays · March 2019

DOI: 10.4006/0836-1398-32.1.112

CITATIONS
13

READS
2,141

2 authors:

Lee Hively
ORNL retired
161 PUBLICATIONS **1,600** CITATIONS
SEE PROFILE

Andrew Loebl
University of Missouri
7 PUBLICATIONS **15** CITATIONS
SEE PROFILE

Classical and extended electrodynamics

Lee M. Hively[1,a)] and Andrew S. Loebl[2]
[1]*4947 Ardley Drive, Colorado Springs, Colorado 80922, USA*
[2]*9325 Briarwood Blvd., Knoxville, Tennessee 39723, USA*

(Received 21 November 2018; accepted 8 February 2019; published online 25 February 2019)

Abstract: Classical electrodynamics is modeled by Maxwell's equations, as a system of eight scalar equations in six unknowns, thus appearing to be overdetermined. The no-magnetic-monopoles equation can be derived from the divergence of Faraday's law, thus reducing the number of independent equations to seven. Derivation of Gauss' law requires an assumption beyond Maxwell's equations, which are then overdetermined as seven equations in six unknowns. This overdetermination causes well-known inconsistencies. Namely, the interface matching condition between two different media is inconsistent for a surface charge and surface current. Also, the irrotational component of the vector potential is gauged away, contrary to experimental measurements. These inconsistencies are resolved by extended electrodynamics (EED), as a *provably unique system of 7 equations in 7 unknowns*. This paper provides new physical insights into EED, along with preliminary experimental results that support the theory. © *2019 Physics Essays Publication*.
[http://dx.doi.org/10.4006/0836-1398-32.1.112]

Résumé: L'électrodynamique classique (CED) est modélisée par les équations de Maxwell, comme un système de 8 équations scalaires dans 6 inconnues, apparaissant ainsi à être surdéterminée. L'équation des monopôles non-magnétiques peut être dérivée de la divergence de la Loi de Faraday, réduisant ainsi le nombre d'équations indépendantes à sept. La dérivation de la Loi de Gauss exige une hypothèse au-delà des équations de Maxwell, qui sont alors surdéterminées comme sept équations dans six inconnues. Cette surdétermination provoque des incohérences bien connues. À savoir, la condition de correspondance d'interface entre deux moyens différents est incohérente pour une charge de surface et un courant de surface. De plus, la composante irrotationnelle du potentiel vectoriel ne peut être mesurée, contrairement aux mesures expérimentales. Ces incohérences sont résolues par l'électrodynamique élargi (EED), *comme un système provablement unique de 7 équations dans 7 inconnues*. Cet article fournit des nouvelles idées physiques sur l'EED, ainsi que des résultats expérimentaux préliminaires qui appuient la théorie.

Key words: General Physics; Classical Field Theory; Electromagnetism; Extended Electrodynamics.

I. INTRODUCTION

Classical electrodynamics (CED) is the cornerstone of modern physics. CED provides the foundation for models of nonlinearity, chaos, complexity, and statistical effects in electrodynamic systems; bioelectrodynamics; polymers; plasmas; conductive fluid dynamics; piezo-electric and piezo-magnetic solids; and computational models thereof.

Maxwell[1] wrote CED as 20 partial differential equations in Cartesian coordinates. Heaviside[2] rewrote Maxwell's equations in vector calculus form with solutions in terms of the scalar (Φ) and vector ($\mathbf{A}$) potentials. Lorenz[3] recognized that wave equations for Φ and $\mathbf{A}$ can be obtained via an additional constraint (the Lorenz gauge). However, the Lorenz gauge does not completely eliminate the arbitrariness in CED, which allows an infinitude of gauge transformations.[4–6]

This paper is inspired by the apparent overdetermination in CED and is organized as follows. Section II summarizes work on CED overdetermination, which is improperly "resolved" by flawed circular logic and unwarranted assumptions. Section III elucidates CED inconsistencies: disparities in the interface matching conditions and gauging away of the gradient component of the vector potential. Section IV introduces extended electrodynamics[7] (EED), together with previous work on EED. Section V gives basic EED predictions: compatibility with CED, resolution of the inconsistencies in Section III, and charge balance in the classical limit. Section VI explains EED prediction of the scalar-longitudinal wave (SLW). Section VII derives the EED conditions for the scalar wave. Section VIII describes the revised energy and momentum balance equations under EED. Section IX discusses preliminary experimental evidence for the SLW: no constraint by the skin effect, $1/r^2$ attenuation in free space, and isotropic SLW transmission from a monopole antenna. Section X provides testable predictions and discussion. Section XI has our conclusions.

a)lee.hively314@comcast.net.us

II. CED OVERDETERMINATION

The vector-calculus form of Maxwell's equations is[8]

$$\nabla \bullet \mathbf{E} = \frac{\rho}{\varepsilon}; \tag{1}$$

$$\nabla \bullet \mathbf{B} = 0; \tag{2}$$

$$\nabla \times \mathbf{E} = -\frac{\partial \mathbf{B}}{\partial t}; \tag{3}$$

$$\nabla \times \mathbf{B} - \mu\varepsilon\frac{\partial \mathbf{E}}{\partial t} = \mu\mathbf{J}. \tag{4}$$

SI units are used. Bold symbols denote vectors; **B** and **E** are the magnetic and electric field vectors, respectively. The source terms are the electric charge density (ρ) and the electrical current density $(\mathbf{J})$; ε and μ are the electrical permittivity and magnetic permeability, respectively (not necessarily vacuum). Time is denoted by t. Equations (1)–(4) seem overdetermined, involving six unknowns (three scalar components for each of **B** and **E**) and eight equations [one from each of Eqs. (1) and (2), and three from each of Eqs. (3) and (4)].

Stratton[9] introduced the divergence-curl redundancy to resolve the overdetermination in CED. Namely, the divergence of Eq. (3) yields[10] $\nabla \bullet \nabla \times \mathbf{E} = 0$. Then, the partial-time derivative of $\nabla \bullet \mathbf{B}$ is zero, which has the solution as $\nabla \bullet \mathbf{B} = \mathrm{F}(\mathbf{r})$, where F is an arbitrary scalar function of spatial location $(\mathbf{r})$. The only physically meaningful result is $\mathrm{F} = 0$, as in Eq. (2). The divergence of Eq. (4) uses[10] $\nabla \bullet \nabla \times \mathbf{B} = 0$ to obtain the form

$$\nabla \bullet \mathbf{E} = -\frac{1}{\varepsilon}\int dt \nabla \bullet \mathbf{J}. \tag{5}$$

Stratton[9] then *assumed* charge conservation, allowing replacement of $\nabla \bullet \mathbf{J}$ in Eq. (5) with the partial-time derivative of $-\rho$, to obtain Eq. (1). While this assumption seems reasonable, Section V describes the first-principles, provably unique derivation of EED[7] that yields a modified form of charge balance. Moreover, charge balance is typically derived by substituting Eq. (1) into the divergence of Eq. (4). Liu[11] noted this circular logic fallacy, but assumed second derivatives in Eqs. (1)–(4) to resolve the overdetermination. Arminjon[12] also addressed this problem, relying on the well-known approach of adding *ad hoc* constraint(s) or dummy variable(s) to the formulation to avoid charge nonconservation.[13–17] These assumptions[9,11,17] hide the fact that *CED is overdetermined*, as Sousa and Shumlak[17] explicitly state.

III. INCONSISTENCIES IN CED

Equations (1) and (2) have well-known solutions,[8] where **A** and Φ are the electrodynamic vector and scalar potentials, respectively,

$$\mathbf{B} = \nabla \times \mathbf{A}; \tag{6}$$

$$\mathbf{E} = -\nabla\Phi - \frac{\partial \mathbf{A}}{\partial t}. \tag{7}$$

Substitution of Eqs. (6) and (7) into Eqs. (1) and (4), and use of the Lorenz gauge, yields the $\Phi-$ and $\mathbf{A}-$ wave equations[8]

$$\nabla^2\Phi - \frac{\partial^2\Phi}{\partial c^2 t^2} = -\frac{\rho}{\varepsilon}; \tag{8}$$

$$\nabla^2\mathbf{A} - \frac{\partial^2\mathbf{A}}{\partial c^2 t^2} = -\mu\mathbf{J}. \tag{9}$$

Here, the speed of light is $c = (\varepsilon\mu)^{-1/2}$ (not necessarily in vacuum). Equation (1) has an interface matching condition[8]

$$\varepsilon_2\mathbf{E}_{2n} - \varepsilon_1\mathbf{E}_{1n} = \rho_A. \tag{10}$$

Substitution of Eq. (7) into Eq. (10) yields

$$\varepsilon_2\left(-\nabla\Phi - \frac{\partial \mathbf{A}}{\partial t}\right)_{2n} - \varepsilon_1\left(-\nabla\Phi - \frac{\partial \mathbf{A}}{\partial t}\right)_{1n} = \rho_A. \tag{11}$$

The subscript, "n," denotes the normal component. The subscripts "1" and "2" identify the two media. Equation (8) also has a matching condition by taking a Gaussian pill box with the end faces parallel to the interface in regions 1 and 2. Noting that $\nabla^2\Phi = \nabla \bullet \nabla\Phi$, one can use the divergence theorem in the limit of zero pill-box height to obtain

$$-(\varepsilon\nabla\Phi)_{2n} + (\varepsilon\nabla\Phi)_{1n} = \rho_A. \tag{12}$$

Here, ρ_A is the surface-charge density at the interface. The discord between Eqs. (11) and (12) is well-known,[18] and is not due to writing the equations in terms of **A** and Φ, since **E** and **B** are gauge invariant.[4–6] Section V resolves this disparity.

The interface matching condition for the tangential component ("t") in Eq. (4) is[8]

$$\mu_1\mathbf{B}_{1t} - \mu_2\mathbf{B}_{2t} = \mu_1(\nabla \times \mathbf{A})_{1t} - \mu_2(\nabla \times \mathbf{A})_{2t} = \mathbf{J}_A. \tag{13}$$

Equation (9) has a matching condition by taking a Gaussian pill box with the end faces parallel to the interface in regions 1 and 2. Noting that $\nabla^2\mathbf{A} = \nabla \bullet \nabla\mathbf{A}$, one can use the divergence theorem in the limit of zero pill-box height to obtain

$$-\left[\frac{(\hat{\mathbf{n}} \bullet \nabla)\mathbf{A}}{\mu}\right]_1 + \left[\frac{(\hat{\mathbf{n}} \bullet \nabla)\mathbf{A}}{\mu}\right]_2 = \mathbf{J}_A. \tag{14}$$

Here, $\mathbf{J}_A$ is the surface-current parallel to the interface; $\hat{\mathbf{n}}$ is the unit vector normal to the interface. As before, the disparity between Eqs. (13) and (14) is not due to writing the equations in terms of **A** and Φ, since **E** and **B** are gauge invariant.[4–6] Section V also resolves this disparity.

Maxwell's equations have an arbitrariness in Φ and **A** for Eqs. (6) and (7), under the transformation[4]

$$\mathbf{A} \to \mathbf{A} + \nabla\Lambda; \tag{15a}$$

$$\Phi \to \Phi - \frac{\partial\Lambda}{\partial t}. \tag{15b}$$

"Gauge" is used to describe Eqs. (15a) and (15b), originally arising from the nonstandard width of railroad track in the 1800 s (a synonym for "arbitrary"). Equations (15a) and (15b) leave **B** and **E** unchanged, which is termed "gauge invariance." A $\aleph_2$-infinitude of choices exists for the gauge function[19] (Λ). For example, the velocity gauge is $\nabla \bullet \mathbf{A} + \beta\varepsilon\mu\partial\Phi/\partial t = 0$. If $\beta = 1$, a charge source propagates at the speed of light (Lorenz gauge). For $\beta = 0$, Φ propagates at infinite speed (Coulomb gauge). For $0 < \beta < 1$, Φ propagates at a speed, c/β. Other conditions are equivalent to the Lorenz gauge with different physical meanings.[5,6]

CED invariance under Eqs. (15a) and (15b) can be cast in four-vector form as $A^\nu \rightarrow A^\nu + \partial^\nu\Lambda$. Here, $A^\nu = (\Phi/c, \mathbf{A})$ and $\partial^\nu = (-\partial/\partial ct, \nabla)$ with a metric signature of (–,+,+,+). Λ is a harmonic, scalar function of space and time that satisfies $\partial_\nu\partial^\nu\Lambda = 0$. Thus, the four-gradient component of A^ν is gauged away under CED.[20,21]

The assumption of no four-gradient in **A** is contrary to experiments that have measured an irrotational vector potential.[22–25] Section VI shows that an irrotational vector potential implies an irrotational current density. Moreover, *an irrotational current* been observed in (for example): arc discharges,[26] ion-concentration-gradient-driven current across living-cell walls,[27] and irrotational, human, electroencephalogram current.[28] This section has demonstrated three inconsistencies in CED: (a) the interface matching condition between two different media is inconsistent at the theoretical level for a surface charge (1) and surface current (2); and (b) the irrotational component of the vector potential is gauged away, contrary to experimental measurements (3). These three inconsistencies may not seem compelling in the light of the success of Maxwell theory in modern physics. However, falsifiability[29] states that a hypothesis (theory) cannot be proved by favorable evidence, but can only be disproved, even by a single failure. These disparities require resolution via EED, as discussed next.

IV. EXTENDED ELECTRODYNAMICS

The Helmholtz theorem[8] uniquely decomposes any three-vector into irrotational and solenoidal parts. For example, electrical current density has the form, $\mathbf{J} = \nabla\kappa + \nabla \times \mathbf{G}$, with κ and **G**, as scalar and vector space-time functions, respectively. Smooth, Minkowski four-vector fields also can be uniquely decomposed into four-irrotational and four-solenoidal parts with tangential and normal components on the bounding three-surface.[30] Woodside[31] subsequently used the Stueckelberg Lagrangian density[32]

$$\mathcal{L} = -\frac{\varepsilon c^2}{4}F_{\mu\nu}F^{\mu\nu} + J_\mu A^\mu - \frac{\gamma\varepsilon c^2}{2}\left(\partial_\mu A^\mu\right)^2 - \frac{\varepsilon c^2 k^2}{2}\left(A_\mu A^\mu\right). \tag{16}$$

$F^{\mu\nu}$ is the Maxwell field tensor; c is the speed of light (not necessarily vacuum); $J_\mu = (c\rho, \mathbf{J})$ is the 4-current; the four-potential is $A_\mu = (\Phi/c, \mathbf{A})$; the Compton wave number for a photon with mass (m) is $k = 2\pi mc/h$; and h is Planck's constant. The fully relativistic Stueckelberg Lagrangian[32] includes both **A** and Φ, and resolves many issues with previous CED Lagrangians. For $\gamma = 0$ and $m > 0$, Eq. (16) yields the Maxwell-Proca theory, for which a 2012 test measured $m \leq 10^{-54}$ kg (equivalent to $\leq 10^{-18}$ eV), consistent with massless photons.[33] Equation (16) for $\gamma = 1$ and $m = 0$ is[31]

$$\mathcal{L} = \frac{\varepsilon c^2}{2}\left[\frac{1}{c^2}\left(\nabla\Phi + \frac{\partial\mathbf{A}}{\partial t}\right)^2 - (\nabla \times \mathbf{A})^2\right] - \rho\Phi + \mathbf{J} \bullet \mathbf{A} - \frac{\varepsilon c^2}{2}\left(\nabla \bullet \mathbf{A} + \frac{1}{c^2}\frac{\partial\Phi}{\partial t}\right)^2. \tag{17}$$

Equation (17) allows only two classes of four-vector fields.[31] One class of fields has zero four-curl of A^μ: $F^{\mu\nu} = \partial^\mu A^\nu - \partial^\nu A^\mu = 0$, with a solution,[31] $A^\mu = \partial^\mu\Lambda$, together with a nonzero, dynamical, scalar field, $C = \partial_\mu A^\mu = \partial_\mu\partial^\mu\Lambda$. Λ is a scalar function of space-time. The second solution[31] has zero four-divergence of A^μ, $C = \partial_\mu A^\mu = 0$, as the Lorenz gauge, consistent with CED.[4] Woodside[7] later *proved the uniqueness* of Eqs. (18)–(22) [7 equations in 7 unknowns $(\mathbf{B}, C, \mathbf{E})$] that form EED:

$$\mathbf{E} = -\nabla\Phi - \frac{\partial\mathbf{A}}{\partial t}; \tag{18}$$

$$\mathbf{B} = \nabla \times \mathbf{A}; \tag{19}$$

$$C = \nabla \bullet \mathbf{A} + \frac{1}{c^2}\frac{\partial\Phi}{\partial t}; \tag{20}$$

$$\nabla \times \mathbf{B} - \frac{1}{c^2}\frac{\partial\mathbf{E}}{\partial t} - \nabla C = \mu\mathbf{J}; \tag{21}$$

$$\nabla \bullet \mathbf{E} + \frac{\partial C}{\partial t} = \frac{\rho}{\varepsilon}. \tag{22}$$

Equation (18) is equivalent to Faraday's law; Eq. (19) is equivalent to the no magnetic-monopoles equation. Equation (21) uniquely decomposes **J** into solenoidal $(\nabla \times \mathbf{B})$ and irrotational (∇C) parts, in accord with the Helmholtz theorem.[8] Equation (17) implies[34] Eqs. (18)–(22). Moreover, Eqs. (18)–(22) imply[7,30,31] Eq. (17). Equation (17) is then necessary and sufficient for Eqs. (18)–(22). The Lagrangian for curved space-time[35] reduces to Eq. (17) in Minkowski four-space.

A long history of work exists on EED.[7,14,30,31,34–44] Fock and Podolsky[36] wrote the new Lagrangian in 1932 with a dynamical, scalar field, $C = \nabla \bullet \mathbf{A} + \varepsilon\mu\partial\Phi/\partial t$, without deriving the resultant equations. Ohmura[37] first wrote the dynamical equations in 1956. Aharonov and Bohm[34] gave the revised Lagrangian and Hamiltonian, and derived the dynamical equations therefrom in 1963. Munz et al.[14] showed the use of EED in computational simulations in 1999. Van Vlaenderen and Waser[38] used EED to derive a wave equation for C, and revised forms for momentum and energy conservation in 2001. Woodside[7,30,31] rigorously derived EED (1999–2009), assuming only Minkowski four-space. Jiménez and Maroto[35] used Eq. (16) with $\gamma = 1$ and $m = 0$ to model quantum, curved space-time, electrodynamics for an expanding universe in 2011. These papers[7,14,30,31,34–38] cited no previous EED work, and serve as seven independent verifications of EED theory.

Modanese[44] studied a nonrelativistic, nonlocal, EED quantum source.

Equations (18)–(22) use the least-action principle,[7] requiring a finite, lower bound on the Lagrangian, Eq. (17). The Planck scale[45] provides such a bound. Another term $-(\nabla \times \mathbf{A})^2/2\mu$, in Eq. (17), has the same requirement for a finite, lower bound, and has been well validated.[4,8]

V. BASIC EED PREDICTIONS

The $\mathbf{B}-$ wave equation arises from the curl of Eq. (21). Note that[10] $\nabla \times \nabla \times \mathbf{B} = \nabla(\nabla \bullet \mathbf{B}) - \nabla^2\mathbf{B}$, which for Eq. (19), $\mathbf{B} = \nabla \times \mathbf{A}$, gives $\nabla \times \nabla \times \mathbf{B} = -\nabla^2\mathbf{B}$. Faraday's law, $\nabla \times \mathbf{E} = -\partial\mathbf{B}/\partial t$, along with[10] $\nabla \times \nabla C = 0$ yields the EED $\mathbf{B}-$ wave equation, identical to CED[8]

$$\nabla^2\mathbf{B} - \frac{\partial^2\mathbf{B}}{\partial c^2 t^2} \equiv \Box^2\mathbf{B} = -\mu\nabla \times \mathbf{J}. \tag{23}$$

The $\mathbf{E}-$ wave equation relies on the equivalence of Eq. (18) to Faraday's law, to which the curl is applied with[10] $\nabla \times \nabla \times \mathbf{E} = \nabla(\nabla \bullet \mathbf{E}) - \nabla^2\mathbf{E}$; replacing $\nabla \times \mathbf{B}$ from Eq. (21); substituting for $\nabla \bullet \mathbf{E}$ via Eq. (22); and noting that $\partial\nabla C/\partial t - \nabla\partial C/\partial t = 0$. The EED $\mathbf{E}-$ wave equation is the CED result[46]

$$\nabla^2\mathbf{E} - \frac{\partial^2\mathbf{E}}{\partial c^2 t^2} = \frac{\nabla\rho}{\varepsilon} + \mu\frac{\partial\mathbf{J}}{\partial t}. \tag{24}$$

The $\mathbf{A}$-wave equation is obtained by: replacing $\mathbf{B}, \mathbf{E}$, and C in Eq. (21) with Eqs. (18)–(20); using the vector calculus identity,[10] $\nabla \times \nabla \times \mathbf{A} = \nabla(\nabla \bullet \mathbf{A}) - \nabla^2\mathbf{A}$; and noting that $\partial\nabla C/\partial t - \nabla\partial C/\partial t = 0$. The result is the CED $\mathbf{A}-$ wave equation,[8] Eq. (9), without the use of a gauge condition.

The $\Phi-$ wave equation can be obtained by: substituting $\mathbf{E}$ and C from Eqs. (18) and (20) into Eq. (22); and noting that $\partial\nabla \bullet \mathbf{A}/\partial t - \nabla \bullet \partial\mathbf{A}/\partial t = 0$. The result is the CED $\Phi-$ wave equation,[8] Eq. (8), without the use of a gauge condition. The usual wave equations for $\mathbf{A}$ and Φ are then rigorously derivable *without a gauge condition*. Thus, EED is gauge-free and predicts the same wave equations for $\mathbf{A}, \mathbf{B}, \mathbf{E}$, and Φ as CED.

Section III described inconsistent interface matching conditions, which are resolved by this gauge-free theory. Namely, Eqs. (21) and (22) are alternative forms of the wave equations for $\mathbf{A}$ and Φ, respectively, as shown above. Thus, the interface boundary conditions for the $\mathbf{A}-$ and $\Phi-$ wave equations are the appropriate forms: Eqs. (12) and (14).

A wave equation for C can be obtained from the divergence of Eq. (21); application of $\varepsilon\mu(\partial/\partial t)$ to Eq. (22); and summing the two results with[10] $\nabla \bullet \nabla \times \mathbf{B} = 0$. The result is[18,38]

$$\nabla^2 C - \frac{\partial^2 C}{\partial c^2 t^2} = -\mu\left(\frac{\partial\rho}{\partial t} + \nabla \bullet \mathbf{J}\right). \tag{25}$$

The rigorous derivation of Eq. (25) eliminates the *ad hoc* assumptions that were described in Section II to avoid the overdetermination of Maxwell's equations.

Equation (25) is an instantaneous equation. But, all experiments are performed over a *finite time,* ΔT, i.e., *a time average*. A long-time average gives $\partial\rho/\partial t + \nabla \bullet \mathbf{J} = 0$ on the right-hand side (RHS) of Eq. (25), in accord with long-standing experiments that validate classical charge balance.[47] For example, the lower bound on electron lifetime for charge balance has been carefully measured as $\geq 6.6 \times 10^{28}$ years[48] (decay into two γ-rays, each at $m_e c^2/2$).

Long-time charge conservation is not inconsistent with charge nonconservation over short-time scales, $\Delta T \leq \Delta t$, per the Heisenberg uncertainty relation, $\Delta E\Delta t \geq \hbar/2$. Here, ΔE is the charged-quantum-fluctuation energy; and $\hbar$ is Planck's constant divided by 2π. Equation (25) can be interpreted as charge nonconservation driving C, and vice versa, not unlike energy fluctuations driving mass fluctuations in quantum theory and vice versa.[18] Thus, Eq. (25) predicts charge conservation on long time-scales (consistent with CED), and exchange of energy between C and quantum fluctuations for $\Delta T \leq \Delta t$. Confirmation of these quantum charge fluctuations involves tests, consistent with the Heisenberg uncertainty relation. One possible test could use the electron $[\Delta E(\text{electron}) = m_e c^2 = 0.51\text{MeV}]$ corresponding to a time, $\Delta t \sim 6 \times 10^{-22}$ s. Subzeptosecond dynamics have been measured,[49] so a direct measurement of this prediction is feasible. Moreover, quantum fluctuations can control charge quantization,[50] in accord with Eq. (25).

The homogeneous solution to Eq. (25) is wavelike, with the lowest-order form in a spherically symmetric geometry,[4] $C = C_o \exp[j(kr - \omega t)]/r$. Here, $j = \sqrt{-1}$; k is the wave number $(2\pi/\lambda)$ for a wavelength, λ; $\omega = 2\pi f$ for a frequency, f; and r is the spherical radius. Boundary conditions for Eq. (25) include $C(r \to \infty) \to 0$, which is trivially satisfied. Equation (44) predicts that the energy density of the $C-$ field is $(C^2/2\mu)$, yielding a constant energy, $4\pi r^2(C^2/2\mu)$, through a spherical boundary around a source in arbitrary media, as required.[18] The interface matching condition for Eq. (25) uses a Gaussian pill box with the end faces parallel to the interface in regions 1 and 2. Noting that $\nabla^2 C = \nabla \bullet \nabla C$, use of the divergence theorem in the limit of zero pill-box height yields continuity in the normal component ('n') of $\nabla C/\mu$ for long times

$$\left(\frac{\nabla C}{\mu}\right)_{1n} = \left(\frac{\nabla C}{\mu}\right)_{2n}. \tag{26}$$

The subscripts, 1 and 2, denote medium 1 and medium 2 for μ not necessarily in vacuum.

VI. EED PREDICTION OF SLW

Section III showed that the four-gradient component of A^ν is gauged away under CED,[20,21] which is inconsistent with experiments.[22–28] Gauge-free EED eliminates this disparity by explicitly including solenoidal (or transverse, denoted by superscript, "T") and irrotational (or longitudinal, denoted by superscript, "L") parts in Eq. (21). Then, a longitudinal vector potential, $\mathbf{A}^L = \nabla\alpha$, yields[10]

$$\mathbf{B} = \nabla \times \mathbf{A}^L = \nabla \times \nabla\alpha = 0, \text{ or } \mathbf{A}^L = \nabla\alpha \Rightarrow \mathbf{B} = 0. \tag{27}$$

Here, α is a scalar function of space-time. The inverse is

$$\begin{aligned} &\mathbf{B}^T = 0 = \nabla \times \mathbf{A}^L \Rightarrow \mathbf{A}^L = \nabla\alpha, \text{ or} \\ &\mathbf{B}^T = 0 \Rightarrow \mathbf{A}^L = \nabla\alpha. \end{aligned} \tag{28}$$

Combining Eqs. (27) and (28) gives

$$\mathbf{A}^L = \nabla\alpha \Longleftrightarrow \mathbf{B}^T = 0. \tag{29}$$

A longitudinal vector potential from Eq. (27) also implies[10]

$$\begin{aligned} \nabla \times \nabla \times \mathbf{A}^L &= \nabla \times \nabla \times \nabla\alpha = 0 \\ &= \nabla(\nabla \bullet \mathbf{A}^L) - \nabla^2\mathbf{A}^L \Rightarrow \nabla(\nabla \bullet \mathbf{A}^L) \\ &= \nabla^2\mathbf{A}^L = \nabla^2\nabla\alpha = \nabla\nabla^2\alpha. \end{aligned} \tag{30}$$

Insertion of Eqs. (29) and (30) into the $\mathbf{A}-$ wave equation gives

$$\begin{aligned} &\Box^2\mathbf{A}^L = \Box^2\nabla\alpha = \nabla\Box^2\alpha = -\mu\mathbf{J} \Rightarrow \mathbf{J}^L = \nabla\kappa, \text{ or} \\ &\mathbf{A}^L = \nabla\alpha \Rightarrow \mathbf{J}^L = \nabla\kappa. \end{aligned} \tag{31}$$

A corollary to Eq. (31), $\nabla\Box^2\alpha = -\mu\nabla\kappa$, is $\Box^2\alpha = -\mu\kappa$. The inverse is also true; $\mathbf{J} = \nabla\kappa + \nabla \times \mathbf{G}^T$ allows decomposition of Eq. (21) into transverse and longitudinal parts

$$\nabla \times \mathbf{B}^T - \frac{1}{c^2}\frac{\partial \mathbf{E}^T}{\partial t} = \mu\nabla \times \mathbf{G}^T \Rightarrow \nabla \times \left(\mathbf{B}^T - \mu\mathbf{G}^T\right) + \frac{\partial^2 \mathbf{A}^T}{\partial c^2 t^2} = 0; \tag{32a}$$

$$-\frac{1}{c^2}\frac{\partial \mathbf{E}^L}{\partial t} - \nabla C = \mu\nabla\kappa \Rightarrow \frac{\partial^2 \mathbf{A}^L}{\partial c^2 t^2} = \nabla\left(-\frac{1}{c^2}\frac{\partial\Phi}{\partial t} + C + \mu\kappa\right). \tag{32b}$$

Rearrangement of Eq. (32b) with substitution of C from Eq. (20) and cancellation of terms, gives the same corollary to Eq. (31) as cited above. Since time and spatial derivatives commute, the right-hand portion of Eq. (32b) results in

$$\mathbf{J}^L = \nabla\kappa \Rightarrow \mathbf{A}^L = \nabla\alpha. \tag{33}$$

Combining Eqs. (31) and (33) yields

$$\mathbf{A}^L = \nabla\alpha \Longleftrightarrow \mathbf{J}^L = \nabla\kappa. \tag{34}$$

The combination of Eqs. (29) and (34) relates $\mathbf{B} = 0$ and $\mathbf{J}^L$

$$\mathbf{J}^L = \nabla\kappa \Longleftrightarrow \mathbf{B}^T = 0. \tag{35}$$

The net result of Eqs. (29), (34), and (35) is

$$\mathbf{A}^L = \nabla\alpha \Longleftrightarrow \mathbf{B}^T = 0 \Longleftrightarrow \mathbf{J}^L = \nabla\kappa. \tag{36}$$

Equation (36) is consistent with the above-cited tests[22–28] and drives the SLW, which is also called an electro-scalar wave.[38,51,52] Clearly, Eq. (36) holds only where $\mathbf{J}$ is nonzero. We prefer the more descriptive phrase, "scalar-longitudinal wave," or SLW, which is used throughout this paper. The explanation for $\mathbf{J}^L$ driving a SLW is as follows. The resultant electric field is $\mathbf{E}^L = \mathbf{J}^L/\sigma = \nabla\kappa/\sigma$ for media with a linear conductivity, σ. $\mathbf{E}^L$ and $\mathbf{J}^L$ for the SLW are curl-free. Faraday's law becomes $\nabla \times \mathbf{E}^L = -\dot{\mathbf{B}} = \nabla \times \nabla\kappa/\sigma = 0$. The overdot denotes a partial-time derivative. Thus, no eddy currents occur, so the SLW is unimpeded by the skin effect for propagation through linearly conductive media. See also Graham *et al.*[53] and Appendix A. C, $\mathbf{E}^L$, and $\mathbf{J}^L$ are all related by Eq. (32b) with[54] $\sigma = \varepsilon_o\varepsilon''\omega$ and $\varepsilon = \varepsilon_o(\varepsilon' - j\varepsilon'')$ for a SLW impedance, Z,

$$Z = \frac{|\mathbf{E}_r|}{|C/\mu_o\mu'|} = \sqrt{\frac{\mu_o}{\varepsilon_o}}\sqrt{\frac{\mu'}{\varepsilon'}}\frac{1 - 1/(jkr)}{1 - j\tan(\delta_\varepsilon)}. \tag{37}$$

Equation (37) assumes spherical waves in linear conductive media: $\mathbf{E}^L = E_r\hat{\mathbf{r}}\exp[j(kr - \omega t)]/r$, together with $C = C_o\exp[j(kr - \omega t)]/r$. The unit vector in the radial direction is $\hat{\mathbf{r}}$; ε_o and μ_o are the free-space permittivity and permeability, respectively; ε' and μ' are the relative permittivity and permeability (not necessarily vacuum), respectively; $\tan(\delta_\varepsilon) = \varepsilon''/\varepsilon'$. Here, the same definitions are used for k, r, t, and ω as in Section V. From Eq. (20), C has the same dimensions as $\mathbf{B} = \mu\mathbf{H}$. Consequently, Eq. (37) uses $|\mathbf{E}|/(C/\mu)$ to obtain the SLW impedance, like the CED form, $Z = |\mathbf{E}|/|\mathbf{H}|$. The $C-$ and $\mathbf{E}-$ field energies from Eq. (44), $4\pi r^2(\varepsilon\mathbf{E}^2/2)$ and $4\pi r^2(C^2/2\mu)$, are constant through a spherical boundary and $C(r \to \infty) = |\mathbf{E}^L(r \to \infty)| \to 0$. Equation (37) predicts $Z_o = \sqrt{\mu_o/\varepsilon_o}$, in free-space ($\varepsilon' = \mu' = 1$ and $\varepsilon'' = \mu'' = 0$). The SLW radiation pattern from a monopole antenna is isotopic, and attenuates as r^{-2} in free space; see Appendix B,

$$\mathbf{P}_{OUT} = \frac{I^2\hat{\mathbf{r}}}{(4\pi r)^2}\sqrt{\frac{\mu}{\varepsilon}}. \tag{38}$$

The SLW has not been previously observed, because transverse electromagnetic (TEM) antennas detect only waves that produce a circulating current. A TEM transmitter produces only circulating currents, yielding $C = 0$ and $\mathbf{E}^L = 0$ with no SLW power output or reception; see Appendix C.

The wave equations for $\mathbf{A}$, $\mathbf{B}$, $\mathbf{E}$, and Φ are unchanged under time reversal. A sign change occurs on both sides of Eq. (25) for $t \to -t$ that also gives time invariance, and indicates the pseudo-scalar nature of C. Time-reversibility of EED implies that reciprocity holds. Then, a SLW transmitter can act as a receiver, and vice versa.

VII. EED PREDICTION OF SCALAR WAVE

EED also predicts a scalar wave (that has *only* a scalar field, and is distinct from the SLW) under the two conditions: $\mathbf{E} = 0$ and Eq. (36).[18] $\mathbf{E} = 0$ corresponds to zero on the left-hand side (LHS) of Eq. (18). Then, the condition ($\mathbf{A}^L = \nabla\alpha$) from Eq. (36) can be combined with the RHS of

Eq. (18) giving $\Phi = -\dot{\alpha}$. Equation (20) for the scalar field can subsequently be rewritten by the replacements, $\Phi = -\dot{\alpha}$ and $\mathbf{A}^L = \nabla\alpha$:

$$C = \nabla \bullet \mathbf{A} + \frac{1}{c^2}\frac{\partial \Phi}{\partial t} = \nabla^2\alpha - \frac{1}{c^2}\frac{\partial^2\alpha}{\partial t} = \Box^2\alpha. \tag{39}$$

Substitution of Eq. (39) into Eq. (25) yields[18]

$$\Box^2\Box^2\alpha = \Box^4\alpha = -\mu\left(\frac{\partial \rho}{\partial t} + \nabla \bullet \mathbf{J}\right). \tag{40}$$

Here, $\Box^2$ is the wave operator as defined in Eq. (23). Use of $\mathbf{E} = 0$ in Eq. (22) yields

$$\frac{\partial C}{\partial t} = \frac{\rho}{\varepsilon} \Rightarrow \rho = \varepsilon\dot{C} = \varepsilon\Box^2\dot{\alpha}. \tag{41}$$

The last form in Eq. (41) comes from the partial-time derivative of Eq. (39). Equation (42) arises from Eq. (40) by replacing $\partial\rho/\partial t$ with the partial-time derivative of Eq. (41), use of $\mathbf{J}^L = \nabla\kappa$ from Eq. (36) to evaluate $\nabla \bullet \mathbf{J}$, and rearrangement of the terms, resulting in the left-hand form

$$\begin{aligned}&\Box^4\alpha + \frac{1}{c^2}\Box^2\ddot{\alpha} + \mu\nabla^2\kappa \\ &= \Box^2\left(\nabla^2\alpha - \frac{\ddot{\alpha}}{c^2} + \frac{\ddot{\alpha}}{c^2}\right) + \mu\nabla^2\kappa \\ &= \nabla^2\left(\Box^2\alpha + \mu\kappa\right) = 0.\end{aligned} \tag{42}$$

The second line of Eq. (42) arises from expansion of the wave operator. The third line of Eq. (42) results from cancellation of the positive and negative $\ddot{\alpha}$-terms along with interchange of the wave- and Laplacian (∇^2) operators, which commute. One solution to Eq. (42) involves setting the term inside the parentheses to zero, which is another form for the longitudinal component of the $\mathbf{A}-$ wave equation [Eq. (9)] with $\mathbf{A}^L = \nabla\alpha$ and $\mathbf{J}^L = \nabla\kappa$. This solution arises, because the gradient and Laplacian operators commute for $\mathbf{A}^L$, per Eq. (30). A second solution to Eq. (42) involves setting the entire left-hand form to zero, which results in the $\mathbf{A}^L-$ wave equation being set equal to a harmonic function[55] $[H(\mathbf{r})e^{j\omega t}]$

$$\Box^2\alpha(\mathbf{r},t) = H(\mathbf{r})e^{jwt} - \mu\kappa(\mathbf{r},t). \tag{42'}$$

Here, the space and time dependences are shown explicitly. $\nabla^2 H(\mathbf{r}) = 0$ is typically solved by separation of variables.[56] For example, in Cartesian coordinates, $H(\mathbf{r})$ involves the sum $H(\mathbf{r}) = \sum X_\xi(x)Y_\psi(y)Z_\zeta(z)$, where $\xi^2 + \psi^2 + \zeta^2 = 0$ and $[X_\xi(x), Y_\psi(y), Z_\zeta(z)]$ are an appropriate set of scalar functions of (x,y,z), respectively. The time-dependent term $(e^{j\omega t})$ that is associated with $H(\mathbf{r})$ is unaffected by the Laplacian operator. Nonhomogeneous solutions to Eq. (42′) are beyond the scope of the present work, being dependent on the specific boundary conditions, geometry, and form for $\kappa(\mathbf{r},t)$. The lowest-order, homogeneous solution to Eq. (42′) is

$$\alpha = \frac{\alpha_o}{r}e^{j(\omega t - kr)}. \tag{43}$$

Substitution of Eq. (43) into Eq. (39) gives the same $1/r$ dependence for C in free space, as for the SLW. Revised energy balance, Eq. (44), shows that the scalar-wave energy is $C^2/2\mu \sim 1/r^2$. Thus, the total scalar-wave energy, $4\pi r^2(C^2/2\mu)$, is constant through a spherical boundary around a source and $C(r \to \infty) \to 0$, as expected. Revised momentum balance, Eq. (45), shows that the scalar wave has a pressure of $\nabla C^2/2\mu$, but no momentum density.

VIII. REVISED BALANCE EQUATIONS

EED predicts a revised energy balance,[18,38] Eq. (44), from the sum of: (C/μ) times Eq. (22); $(\mathbf{B}/\mu)\bullet$ applied to Faraday's law; and application of $-(\mathbf{E}/\mu)\bullet$ applied to Eq. (21)

$$\begin{aligned}&\frac{\partial}{\partial t}\left(\frac{\mathbf{B}^2}{2\mu} + \frac{C^2}{2\mu} + \varepsilon\mathbf{E}^2\right) + \nabla \bullet \left(\frac{\mathbf{E}\times\mathbf{B}}{\mu} + \frac{C\mathbf{E}}{\mu}\right) \\ &\quad + \mathbf{J} \bullet \mathbf{E} = \frac{\rho C}{\varepsilon\mu}.\end{aligned} \tag{44}$$

Equation (44) has new energy density terms: scalar field energy $(C^2/2\mu)$, SLW energy $(C\mathbf{E}/\mu)$, and a power source $(\rho C/\varepsilon\mu)$.

EED predicts revised momentum balance,[18,38] Eq. (45), as the sum of: $(\mathbf{B}/\mu)\nabla \bullet \mathbf{B} = 0$; the cross product of $(\varepsilon\mathbf{E})$ with Faraday's law; Eq. (21) $\times(-\mathbf{B}/\mu)$; $(C/\mu)\times$ Eq. (21); and $(-\varepsilon\mathbf{E})\times$ Eq. (22). Equation (45) has new density terms: SLW momentum flux $(C\mathbf{E}/\mu)$, TEM-SLW mixed mode flux $[(\nabla\times\mathbf{B}C)/\mu]$, a force $(\mathbf{J}C)$ parallel to the current density, and scalar-field pressure $(\nabla C^2/2\mu)$. The last term in Eq. (45) is the divergence of the CED Maxwell stress tensor[4]

$$\begin{aligned}&\varepsilon\mu\frac{\partial}{\partial t}\left(\frac{\mathbf{E}\times\mathbf{B}}{\mu} - \frac{C\mathbf{E}}{\mu}\right) + \rho\mathbf{E} + \mathbf{J}\times\mathbf{B} + \frac{\nabla\times\mathbf{B}C}{\mu} \\ &\quad = \mathbf{J}C + \frac{\nabla C^2}{2\mu} + \nabla \bullet \vec{\mathbf{T}}\,.\end{aligned} \tag{45}$$

Equation (44) predicts a power *gain* $(+C\mathbf{E}/\mu)$ with momentum *loss* $(-C\mathbf{E}/\mu)$ in Eq. (45), and vice versa. This sign difference means that a SLW emission (power *loss*) drives a momentum *gain* in a massive object that emits the SLW.

IX. PRELIMINARY SLW EXPERIMENTS

The present work eliminates sources of error in previous tests,[51,52] which are discussed in Appendix D. High frequency (~8 GHz) experiments facilitate an indoor, controlled test environment. Figure 1 shows the test layout. The transmitter and receiver are identical (inverted triangles in the lower left of Fig. 1), since time-reversal symmetry allows the transmitter to act as a receiver, as discussed in Section VI. The directional couplers act as 45-dB isolators. Grounding to a single point avoids current loops. Modern digital instrumentation allows accurate measurement of signal amplitudes and distances for comparison of test results to EED predictions.

Figure 2 shows the linear, monopolar, SLW antenna with the coaxial center conductor as the radiator. The outer

Item	Make/Model/Description	#	Connectors
1)Pre-amplifier	IFI T186-50 TWT (50W, 6-18GHz)	1	Nf-Nf
2)Network analyzer	Agilent E5071C (151dB dynamic range)	1	Nf-Nf
3)Calibration kit	Agilent N6314A Type n	1	N
4)Wave attenuator	Minicircuits FW-20+ (1W, 20dB)	3	SMAm-SMAf
5)Directional coupler	Fairfield MW MC0412-30 (50W, 30dB)	2	SMAf (all)
6)Rotary positioner	Newmark RT-3-10 rotary stage	1	n/a
7)Linear positioner	Newmark EB-1500-1 linear stage	1	n/a
8)Stage controller	Newmark NSC-G2 stage controller	1	n/a
RG-405/U cable	3' length	1	N-male to N-male
RG-405/U cable	1' length	1	N-male to SMA-male
RG-405/U cable	2' length	3	SMA-male to SMA-male
RG-405/U cable	6" length	1	SMA-male to SMA-male
RG-405/U cable	5' length	1	SMA-female to N-male
RG-405/U cable	5' length; straight SMA plug to …	8	straight SMA female jack
RG-405/U cable	2' length; straight SMA plug to …	3	straight SMA female jack

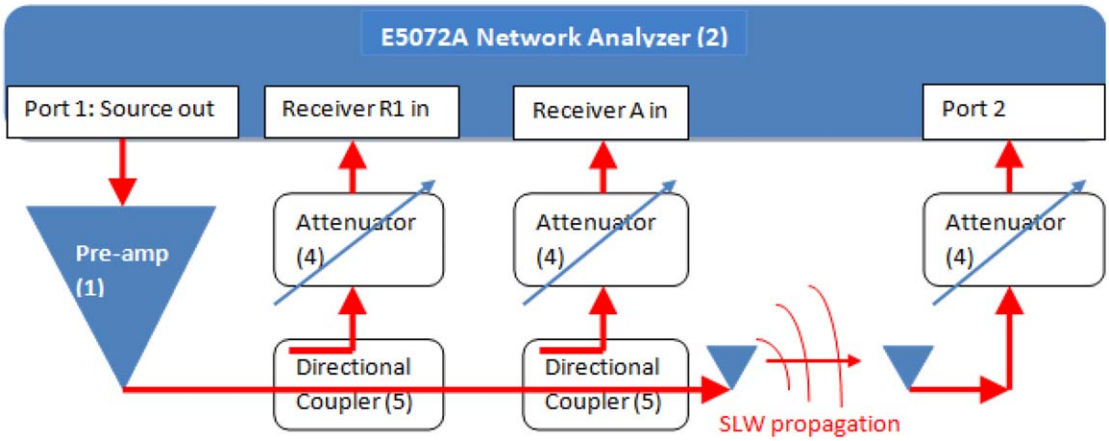

FIG. 1. (Color online) Test layout, with numbered items in the diagram corresponding to the tabular description above. This figure does not show Items 3, and 6–8, which are discussed in the text.

coaxial conductor is electrically connected to the top of the skirt balun.[57,58] The skirt balun length $(\lambda/4)$ causes a phase shift in the current flow along the guided path from the bottom (inside surface) of the skirt balun conductor (0°) to the top (inside surface) of the skirt balun (90°) and back down the outer surface of the coax outer conductor to the end of the skirt balun (180°). The 180°-phase shift attenuates the return current along the outside of the outer coaxial conductor to form a monopole antenna, thus eliminating the image charge and image current of previous tests.[51,52] The resultant far-field contours of constant $|\mathbf{E}|$ from an HFSS electrodynamic simulation are essentially spherical, as expected for a monopolar antenna (top of Fig. 2). The RG-405/U coaxial cabling uses a solid, outer conductor to minimize stray fields; the presence or absence of an outer insulating jacket makes no difference in the results of the electrodynamic simulation. (A 3λ-diameter ground-plane disk at the feed-point gives essentially the same $|\mathbf{E}|$ contours, thus confirming the linear monopolar, counter-poise design.)

The return-current attenuation (23 dB) of the previous paragraph is quantified in Fig. 3, as a sharp null at 7.94 GHz (shown in red online). Return-current attenuation allows the monopole antenna to draw charge from the ground plane (top of the skirt balun) and also creates an impedance match between the antenna-balun (49.76–j0.24 Ω) and the source (50 Ω). Thus, the skirt balun reduces the return current along the outside of the outer coax conductor, so that essentially all of the electrical current goes into charging and discharging the antenna (an irrotational current) to drive the SLW, as predicted in Eq. (36). The test result for a single skirt balun (shown in green online in Fig. 3) shows the same trend as the HFSS simulation with a minimum of −23 dB at 8.00 GHz; the test result for a double balun was −42 dB (not shown). The difference in null depth arises from inaccuracies in the antenna fabrication. Variation in the return loss with frequency arises from the tuned balun geometry.

One experiment tested two critical EED predictions. Namely, the SLW is unconstrained by the skin effect, and the free-space attenuation of the SLW has a $1/r^2-$ dependence. The test measured signal attenuation (dB) versus distance (r) with the transmitting-antenna location fixed, and the receiving antenna moved in a straight line horizontally via a linear positioner with 1-mm accuracy. The source frequency was 8.00 GHz with a free-space wavelength,

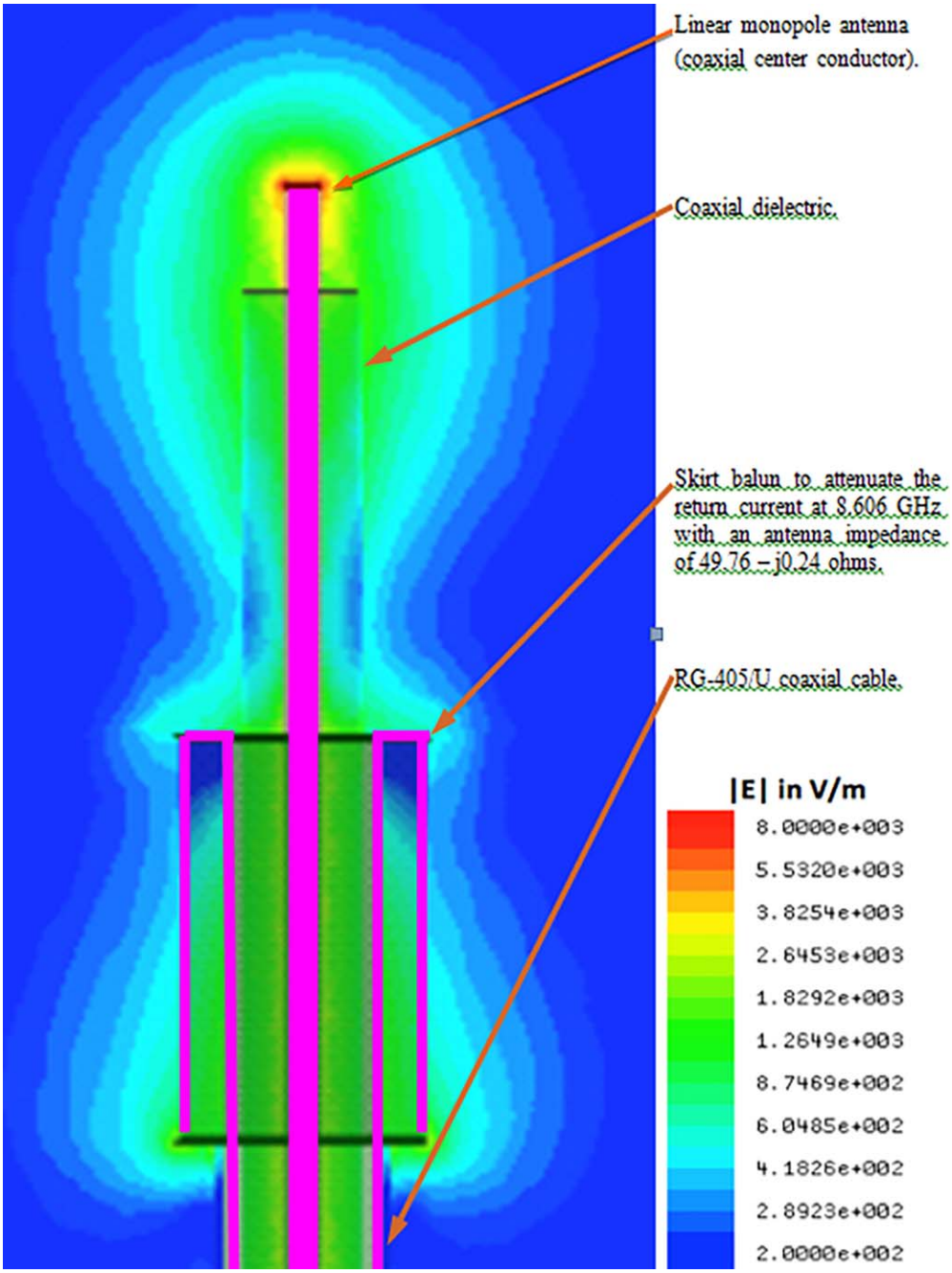

FIG. 2. (Color online) Cross-sectional view of constant |**E**| contours for the SLW antenna. Heavy lines (shown in purple online) are conductors for the linear monopole antenna (top label), skirt balun (middle label), and outer conductor of the coaxial cable (bottom label).

$\lambda = 3.75$ cm. Figure 4 shows the results for two, facing, collinear SLW-antennas inside an anechoic, Faraday chamber (90 dB isolation).

In addition, each antenna was inside its own separate Faraday enclosure. Each antenna enclosure consisted of a copper pipe (Nibco copper coupling without C x C – Wrot, 601) and two hemispherical end caps (outer diameter = 15.85 mm, inner diameter = 14.34 mm). The pipe length was 28.89 mm with a wall thickness of 1.02 mm. The hemispherical end caps (Nibco Cap C – Wrot, 617) had an outer diameter of 17.80 mm, an inner diameter of 15.80 mm, and a wall thickness of 1.05 mm. One end cap had a central hole slightly larger than the outer diameter of the coaxial outer conductor. This end cap was carefully soldered to the coax outer conductor to create a strong structural bond and a tight, 360° electrical seal between the Faraday enclosure and the coax outer conductor. Likewise, the hemispherical caps were soldered to each end of the copper pipe to create a strong structural bond and a tight, 360° electrical seal. Figure 4 shows the SLW signal attenuation through both antenna enclosures. The straight-line, least-squares-fit, log-log slopes are −2.6301 and −2.2273 for the top and bottom plots, respectively. The measurements are presently too noisy to distinguish these slopes from −2. The interior of the Faraday enclosures for each antenna did not have any RF attenuating foam, allowing resonance-cavity effects that are not included

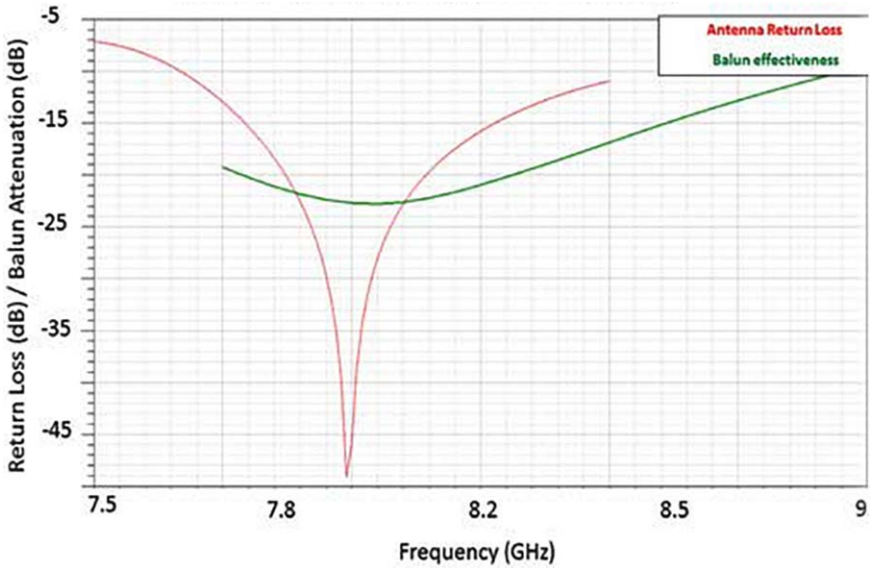

FIG. 3. (Color online) Attenuation of the return current as a function of frequency, showing a minimum in the HFSS-model results with a sharp null to −49 dB at 7.94 GHz (shown in red online) in comparison to the measured balun effectiveness with a shallow null to −23 dB at 8.00 GHz (shown in green online).

in the present theory. SLW attenuation in conductive media is the subject of future work. The combined solid-copper thickness (2×1.02 mm) is 2914 skin depths in the result of Fig. 4, which should produce a classical attenuation of $\sim 10^{-1265}$ in TEM waves. The test measurement yielded an attenuation between −115 dB at $r = 2$ cm separation and −137 dB at $r = 30$ cm. Extrapolating the straight-line fit to a separation of 2 mm (where the enclosed antennas are barely separated) gives −79 dB and −86 dB, for an attenuation of $\sim 10^{-4}$. The difference between the measured value and the

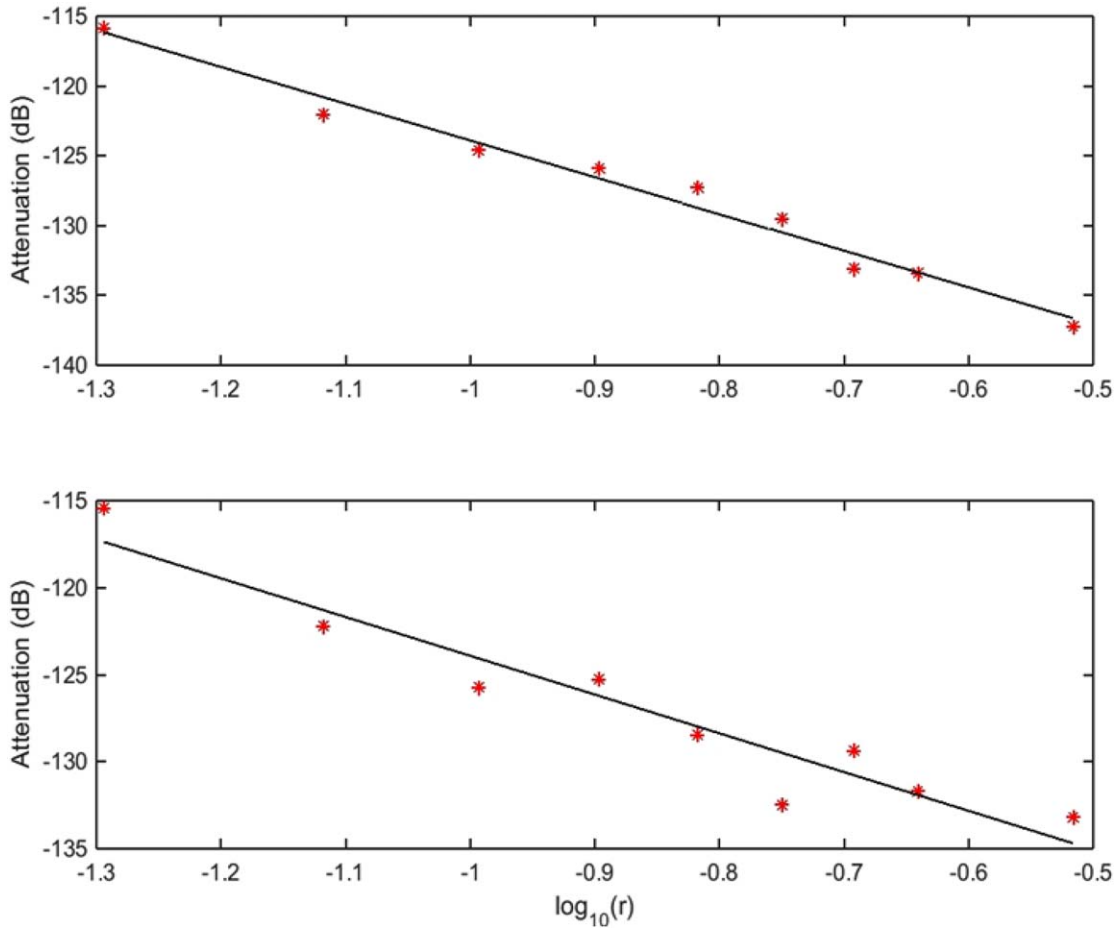

FIG. 4. (Color online) SLW attenuation (S21 in the top plot and S12 in the bottom plot) in dB versus the transmitter-to-receiver distance in r (meters).

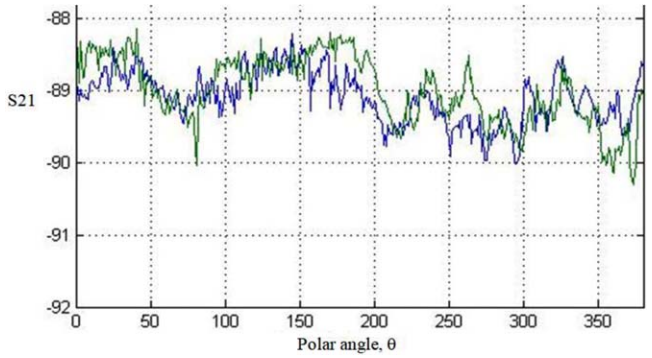

FIG. 5. (Color online) SLW power variation (dB) versus polar angle (θ) for a bare SLW antenna (transmitter) and a Faraday-boxed SLW antenna (receiver). Two repetitions of the test (green and blue) show reproducibility within ± 1 dB.

classical prediction is >1261 orders of magnitude. This disparity far exceeds the criterion for a scientific discovery (five standard deviations or a probability of $<3 \times 10^{-7}$). These results show that the SLW is unconstrained by the skin effect with $1/r^2-$ attenuation in free-space. These results are consistent with EED and cannot be explained by CED.

The extraordinary result in the previous paragraphs requires substantial discussion. We emphasize that the above results are from *preliminary* measurements and may have confounding factors that have yet to be identified. One issue may be TEM signals being picked up by the coaxial cables, either inside or outside the Faraday cage. This issue was addressed by the use of RG405/U cables with a solid copper outer conductor everywhere, which eliminated TEM interference. In this light, we did not use a TEM receiving antenna inside the Faraday cage to confirm the absence of such a signal. A second issue is that the SLW is unconstrained by the skin effect (Appendix A) and can therefore penetrate the solid copper outer conductor of the RG405/U cabling, which moved with the motion of the linear and rotational positioners. This cable motion probably accounts for the large variability in the results of Figs. 4 and 5. A third issue is the distance between the transmitter and receiver in comparison to the wavelength, Namely, a longitudinal **E**-field component occurs in the near-field under classical (Maxwell) electrodynamics at a distance of $\leq 3\lambda$ for the largest dimension of the antenna small in comparison to the wavelength.[59] However, a significant signal was received 30 cm (8 wavelengths) from the transmitter, which is well beyond the near-field. Moreover, detection of this far-field signal required the SLW to penetrate a 1-mm thick Faraday enclosure that surrounded the transmitter, as well as a 1-mm thick Faraday enclosure around the receiver. Wave penetration of the two 1-mm thick Faraday enclosures (2-mm total) demonstrates the low-loss nature of the SLW in conductive media. A more accurate and compelling result clearly requires a much better experimental design, which is the subject of future work.

Equation (38) predicts isotropic transmission from the SLW monopole antenna. Figure 5 shows the variation between a bare, single-balun transmitter and a Faraday-enclosed, single-balun receiver with a fixed separation of $r = 0.75$ m. Both antenna axes were in the horizontal plane inside the anechoic Faraday chamber. The receiving antenna was rotated 360° in the horizontal plane (polar angle, θ) by a rotational positioner in 1° increments. The variability over the entire angular range is ± 1 dB, showing isotropy within the measurement accuracy from the linear, monopole antenna, in accord with the EED prediction.

X. DISCUSSION

EED allows spherical symmetry, Eq. (38), in the electrical current density (**J**) and longitudinal fields, which CED forbids.[60] Table I shows testable EED predictions. Starred items in Table I are consistent with tests in Section IX. The star for

TABLE I. Summary of testable EED predictions.

Item	Brief description of testable prediction	Reference
1	The interface matching condition for ρ_A is…	Equation (12)
2	The interface matching condition for $\mathbf{J}_A$ is…	Equation (14)
3	The SLW has a scalar field, $C = \nabla \bullet \mathbf{A} + \varepsilon\mu\partial\Phi/\partial t$.	Equation (20)
4	The scalar field is also charge-fluctuation driven.	Equation (25)
5	The interface matching condition for C is…	Equation (26)
6	The SLW has drivers: $\mathbf{A}^L = \nabla\alpha \Longleftrightarrow \mathbf{B}^T = 0 \Longleftrightarrow \mathbf{J}^L = \nabla\kappa$.	Equation (36)*
7	The SLW has a longitudinal $\mathbf{E}-$ field.	Section VI
8	The SLW is unconstrained by the skin effect.	Section VI*
9	C is a pseudo-scalar field.	Section VI
10	The SLW has a power comparable to the TEM wave.	Equation (37)*
11	The SLW free-space attenuation goes like $1/r^2$.	Equation (38)*
12	The SLW monopole radiation is isotropic.	Equation (38)*
13	The scalar wave arises from $\Phi = -\dot{\alpha}$ and…	Equation (42)
14	The scalar-field energy density is $C^2/2\mu$.	Equation (44)
15	The SLW power density vector is $C\mathbf{E}/\mu$.	Equation (44)
16	Energy balance has a new source, $\rho C/\varepsilon\mu$.	Equation (44)
17	The SLW momentum density is $-C\mathbf{E}/\mu$.	Equation (45)
18	Momentum balance has a mixed-mode term, $\nabla \times \mathbf{B}C/\mu$.	Equation (45)
19	Momentum balance also has source term, $\mathbf{J}C$.	Equation (45)
20	The scalar-field pressure density is $\nabla C^2/2\mu$.	Equation (45)

Item 6 occurs, because the linear, monopolar SLW antenna with a balun imposes an irrotational current, as discussed in Section IX. The star for Item 10 arises, because the SLW attenuation is measured with standard instrumentation and has a free-space impedance that is identical to TEM waves.

Haag's theorem[61] states that two Hilbert solutions may be unitarily inequivalent within quantum field theory (QFT). The "proper" representation must then be chosen from an infinite set of inequivalent forms. Seidewitz[62] showed that Haag's theorem does not apply to Eq. (16). Equations (18)–(22) are a necessary and sufficient condition for Eq. (16) with $\gamma = 1$ and $m = 0$, resolving the problem of inequivalent unitary QFT forms. We note that the relativistic field equations arising from the Stueckelberg Lagrangian[32] are taught in advanced physics texts, e.g., Ref. 63.

XI. CONCLUSIONS

The conclusions of this work follow. Section II shows that CED is overdetermined. Section III identifies inconsistencies in CED that arise from this overdetermination: incorrect interface matching conditions and gauging away of the four-gradient in A^{ν}. Section IV shows the provably unique basis for EED,[7] which has a new term (∇C) in Ampere's law and a new term $(\partial C/\partial t)$ in Gauss' law. Section V rigorously derives the CED wave equations from EED without a gauge condition. EED also eliminates the inconsistencies that are identified in Section III, and predicts a revised form for charge conservation without any *ad hoc* assumption(s). In Section VI, EED further predicts a free-space, SLW. Equation (36) shows that the SLW arises from an irrotational current, a longitudinal vector potential, or antennas that have a null magnetic field. Section VII derives the conditions for a scalar wave under EED. Section VIII shows the EED derivation of revised energy and momentum balance. Section IX presents preliminary experimental results for the SLW (five of the testable predictions in Table I) that are consistent with EED and cannot be explained by CED. Specifically, the tests show that the SLW: (a) is unconstrained by the skin effect via propagation through Faraday enclosures with a disparity of *1261 orders of magnitude* between CED and EED; (b) can be transmitted and received by a monopolar antenna (not to be confused with magnetic monopoles) with an isotropic radiation pattern; and (c) has a free-space attenuation consistent with $1/r^2$. The disparity under item (a) far exceeds the criterion for a scientific discovery {five standard deviations [probability $\leq 3 \times 10^{-7}$($\sim$7.5 orders of magnitude)]. These measurements are in accord with the EED theory developed in Sections V and VI. Clearly, much additional work is needed to strengthen and replicate these measurements.

ACKNOWLEDGMENTS

Insightful suggestions by Aly Fathy, David Fugate, David Froning, George Hathaway, Roger Kisner, Giovanni Modanese, Mike Pascale, Theophanes Raptis, Donald Reed, Igor Smolyaninov, John Wilgen, and Dale Woodside are gratefully acknowledged. Additional comments by two anonymous reviewers led to changes that substantially strengthened this essay. Professor Aly Fathy kindly provided the use of his experimental equipment and facility at the University of Tennessee (Knoxville). LMH did the theoretical analysis, wrote the paper, designed the experiments, and analyzed test results; ASL performed the tests and provided numerous editorial comments. This work was partially funded by ScalarWave LLC, and its successor (Gradient Dynamics, LLC), a privately owned, Delaware company. Further details are disclosed in US Patent #9,306,527 by the first author, dated 05 April 2016.

APPENDIX A: SLW IN CONDUCTIVE MEDIA

A necessary and sufficient condition for the SLW, Eq. (36), is $\mathbf{B} = 0$, which gives $\Box^2\mathbf{B} = -\mu\nabla \times \mathbf{J} = 0$. The curl of the (RHS) of this last equation is[10] $\nabla \times \nabla \times \mathbf{J} = \nabla(\nabla \bullet \mathbf{J}) - \nabla^2\mathbf{J} = 0$. The resultant form is

$$\nabla(\nabla \bullet \mathbf{J}) = \nabla^2\mathbf{J}. \tag{A1}$$

The gradient of the classical charge-conservation equation with substitution from Eq. (A1) yields

$$\frac{\partial \nabla \rho}{\partial t} = -\nabla\left(\nabla \bullet \mathbf{J}\right) = -\nabla^2\mathbf{J}. \tag{A2}$$

The partial time-derivative of the **E**-wave equation, Eq. (24), with substitution from Eq. (A2) is

$$\Box^2\dot{\mathbf{E}} = \mu\frac{\partial^2\mathbf{J}}{\partial t^2} + \frac{1}{\varepsilon}\frac{\partial \nabla \rho}{\partial t} = \mu\frac{\partial^2\mathbf{J}}{\partial t^2} - \frac{\nabla^2\mathbf{J}}{\varepsilon} = \frac{\Box^2\mathbf{J}}{\varepsilon}. \tag{A3}$$

Equation (A3) can be rewritten, using Ohm's law, $\mathbf{J} = \sigma\mathbf{E}$, for linearly conductive media

$$\Box^2\left(\dot{\mathbf{E}} + \frac{\mathbf{J}}{\varepsilon}\right) = \Box^2\left(\dot{\mathbf{E}} + \frac{\sigma\mathbf{E}}{\varepsilon}\right). \tag{A4}$$

One solution to Eq. (A4) sets the terms inside the parentheses to zero, as a transient solution[4] that typically decays in $\sim 10^{-19}$s

$$\mathbf{E} = \mathbf{E_o}e^{-\varepsilon t/\sigma}. \tag{A5}$$

$\mathbf{E}_o$ in Eq. (A5) is the initial value of **E**. A second solution to Eq. (A4) uses the nontransient, separable form for **E** after the transient decay

$$\mathbf{E} = \mathbf{E_o}(\mathbf{r})e^{-j\omega t}. \tag{A6}$$

Here, **r** is the position vector. Substitution of Eq. (A6) into Eq. (A4) with elimination of common terms gives

$$\Box^2\mathbf{E} = 0. \tag{A7}$$

The lack of a source term on the RHS of Eq. (A7) means that the SLW propagates without loss in isotropic, homogeneous conductive media (σ = constant). That is, the SLW is unconstrained by the skin effect. This prediction can be verified by substitution of the spherical wave forms for **E** and C into the energy balance equation, Eq. (44), with $\mathbf{B} = 0$ and the ratio of $|\mathbf{E}_r|/|C/\mu|$ from Eq. (37); the same result arises for plane waves.

APPENDIX B: SLW TRANSMISSION POWER

The SLW power output ($\mathbf{P}_{OUT}$) is obtained via the method in Chapter 9 of Jackson.[4] A linear, thin-wire antenna is assumed on the z-axis over the interval, $0 \le z \le L \le \lambda \ll r$. $\mathbf{J}$ and ρ are initially written in Cartesian coordinates

$$\mathbf{J}^L = \frac{\hat{\mathbf{z}} I\delta(x)\delta(y)e^{-j\omega t}(\cos kz - \cos kL)}{(1 - \cos kL)}. \tag{B1}$$

$$\rho = \frac{jI\delta(x)\delta(y)e^{-j\omega t}\sin kz}{c(1 - \cos kL)}. \tag{B2}$$

The irrotational current density ($\mathbf{J}^L$) is maximal at the feed point, $z = 0$ (where the center conductor exits the coaxial cable), and zero at the end of the antenna ($z = L$). The Dirac delta function is denoted by $\delta(\ldots)$; the current is I. The charge density (ρ) is determined from $\mathbf{J}$ by classical charge balance. Φ and $\mathbf{A}$ are obtained by Green's-function solutions to Eqs. (8) and (9)

$$\Phi = \frac{Ie^{j(kr-\omega t)}}{4\pi c\varepsilon kr(1 - \cos kL)} \times \left[\frac{e^{-jkL\cos\theta}(-j\cos kL + \cos\theta\sin kL) + j}{\sin^2\theta}\right]; \tag{B3a}$$

$$\mathbf{A} = \frac{\mu I\hat{\mathbf{z}}e^{j(kr-\omega t)}}{4\pi kr(1 - \cos kL)} \times \left[\frac{e^{-jkL\cos\theta}(\sin kL - j\cos\theta\cos kL) + j\cos\theta}{\sin^2\theta} - \frac{j\cos kL}{\cos\theta}(e^{-jkL\cos\theta} - 1)\right]. \tag{B3b}$$

Equations (B3a) and (B3b) are now written in cylindrical coordinates. As before, ε and μ are the permittivity and permeability of the propagation medium, respectively, (not necessarily vacuum). Equations (B3a) and (B3b) assume $kL \le 1$ (small antenna) and $kr \gg 1$ (far field), allowing terms on the order of $(kr)^{-1}$ and higher to be neglected in comparison to unity. C and $\mathbf{E}$ then are obtained from Eqs. (18) and (20) in spherical coordinates with $\hat{\mathbf{z}} = \hat{\mathbf{r}}\cos\theta - \hat{\boldsymbol{\theta}}\sin\theta$:

$$C = \nabla \bullet \mathbf{A} + \frac{1}{c^2}\frac{\partial\Phi}{\partial t} = \frac{\mu Ie^{j(kr-\omega t)}}{4\pi r}; \tag{B4a}$$

$$\mathbf{E} = -\nabla\Phi - \frac{\partial\mathbf{A}}{\partial t} = \frac{c\mu Ie^{j(kr-\omega t)}\left[\hat{\mathbf{r}} - \hat{\boldsymbol{\theta}}f(\theta)\right]}{4\pi r}. \tag{B4b}$$

Equation (B4b) has $f(\theta)$, which is irrelevant to this derivation, because the radiated power flows only in the radially outward ($+\hat{\mathbf{r}}$) direction). $\mathbf{P}_{OUT}$ for the SLW is determined from the time-averaged, radial component, $<C^*\mathbf{E}/\mu>$ from Eq. (44)

$$\mathbf{P_{OUT}} = \frac{I^2\hat{\mathbf{r}}}{(4\pi r)^2}\sqrt{\frac{\mu}{\varepsilon}}. \tag{B5}$$

APPENDIX C: SLW FROM TEM ANTENNA

The SLW power output ($\mathbf{P}_{OUT}$) is obtained by the procedure in Chapter 9 of Jackson.[4] A linear, thin-wire, dipolar antenna is assumed along the z-axis over the interval, $-L \le z \le L \le \lambda \ll r$. The current ($\mathbf{J}$) and charge densities ($\rho$) are the same as in Appendix B; the notation is also identical to Appendix B. Φ and $\mathbf{A}$ are obtained from the Green's-function solutions to Eqs. (8) and (9)

$$\mathbf{A} = \frac{\mu I\hat{\mathbf{z}}e^{j(kr-\omega t)}}{2\pi kr} \times \left[\frac{\sin kL\cos(kL\cos\theta)\cos\theta - \cos kL\sin(kL\cos\theta)}{(1 - \cos kL)\sin^2\theta\cos\theta}\right]; \tag{C1a}$$

$$\Phi = \frac{Ie^{j(kr-\omega t)}}{2\pi\varepsilon\omega r} \times \left[\frac{\sin kL\cos(kL\cos\theta)\cos\theta - \cos kL\sin(kL\cos\theta)}{(1 - \cos kL)\sin^2\theta}\right]. \tag{C1b}$$

Equations (C1a) and (C1b) are written in cylindrical coordinates. As in Appendix B, ε and μ are the permittivity and permeability of the propagation medium, respectively, (not necessarily vacuum). Equations (C1) assume $kL \le 1$ (small antenna) and $kr \gg 1$ (far field), allowing terms on the order of $(kr)^{-1}$ and higher to be neglected in comparison to unity. C is then obtained from Eqs. (C1) with $\hat{\mathbf{z}} = \hat{\mathbf{r}}\cos\theta - \hat{\boldsymbol{\theta}}\sin\theta$, using spherical coordinates on the RHS

$$C = \nabla \bullet \mathbf{A} + \frac{1}{c^2}\frac{\partial\Phi}{\partial t} = \frac{1}{r^2}\frac{\partial(r^2\mathbf{A}_r)}{\partial r} + \frac{1}{c^2}\frac{\partial\Phi}{\partial t}. \tag{C2}$$

The resultant expression in the far-field for C becomes

$$C = \frac{(1-1)j\mu Ie^{j(kr-\omega t)}}{2\pi r} \times \left[\frac{\sin kL\cos(kL\cos\theta)\cos\theta - \cos kL\sin(kL\cos\theta)}{(1-\cos kL)\sin^2\theta}\right] = 0. \tag{C3}$$

Moreover, the radial component of $\mathbf{E}$ in the far field is

$$\mathbf{E} = \frac{(1-1)jI\hat{\mathbf{r}}e^{j(kr-\omega t)}}{2\pi r}\sqrt{\frac{\mu}{\varepsilon}} \times \left[\frac{\sin kL\cos(kL\cos\theta)\cos\theta - \cos kL\sin(kL\cos\theta)}{(1-\cos kL)\sin^2\theta}\right] = 0. \tag{C4}$$

Consequently, $\mathbf{P}_{OUT}(\mathrm{SLW}) = <C^*\mathbf{E}/\mu>$ is zero. This result explains the nondetection of the SLW by TEM antennas, which can detect waves that generate only a circulating

current (no gradient-driven current). Again using $\hat{\mathbf{z}} = \hat{\mathbf{r}}\cos\theta - \hat{\boldsymbol{\theta}}\sin\theta$ for TEM waves, the theta-component of $\mathbf{E}$ from Eq. (18) is

$$\mathbf{E} = \frac{-jI\hat{\boldsymbol{\theta}}e^{j(kr-\omega t)}}{2\pi r}\sqrt{\frac{\mu}{\varepsilon}} \times \left[\frac{\sin kL\cos(kL\cos\theta)\cos\theta - \cos kL\sin(kL\cos\theta)}{(1-\cos kL)\sin\theta\cos\theta}\right]. \tag{C5}$$

The magnetic field from the TEM antenna from Eq. (19) is

$$\mathbf{B} = \frac{-j\mu I\hat{\boldsymbol{\varphi}}e^{j(kr-\omega t)}}{2\pi r} \times \left[\frac{\sin kL\cos(kL\cos\theta)\cos\theta - \cos kL\sin(kL\cos\theta)}{(1-\cos kL)\sin\theta\cos\theta}\right]. \tag{C6}$$

$\mathbf{P}_{OUT}$ (TEM)$= <\mathbf{E}^* \times \mathbf{B}/\mu >$ for the TEM wave then is

$$\mathbf{P}_{OUT} = \frac{I^2\hat{\mathbf{r}}}{(2\pi r)^2} \times \left[\frac{\sin kL\cos(kL\cos\theta)\cos\theta - \cos kL\sin(kL\cos\theta)}{(1-\cos kL)\sin\theta\cos\theta}\right]^2. \tag{C7}$$

Equation (C7) is zero in the limits of $\theta \to 0, \pi$ via L'Hospital's rule. $\mathbf{P}_{OUT}$ is maximal for $\theta \to \pi/2$ via L'Hospital's rule

$$\mathbf{P_{OUT}} = \frac{I^2\hat{\mathbf{r}}}{(2\pi r)^2}\left[\frac{kL\cos(kL) - \sin(kL)}{(1-\cos kL)}\right]^2. \tag{C8}$$

Equations (C7) and (C8) are consistent with Jackson's Eq. (9.28), which assumed a constant current density, rather than a more realistic sinusoidal current density,[4] as done here.

APPENDIX D: DISCUSSION OF PREVIOUS SLW TESTS

A test by Monstein and Wesley[51] used a 6-cm diameter, center-fed aluminum spherical transmitter and receiver at 433.59 MHz ($\lambda = 69.2$ cm). A three-by-three array of half-wavelength, linear, electric-dipole antennas was placed between the transmitter and receiver. The signal was strongly attenuated for the dipole-array parallel to the transmitter-receiver direction. No attenuation occurred for an array orientation perpendicular to the propagation direction, showing that the $\mathbf{E}-$ wave polarization was *longitudinal*. The results agreed with image-charge theory for separation distances less than 100 m (144 wavelengths), including two interference minima. The outdoor tests were performed near the bank of the Rhein River in Switzerland. The outer conductor of the coaxial cable was grounded, inducing unquantified electrical ground currents. The transmitter-receiver distance was measured via GPS (accuracy of $\pm$5m). Bray and Britton[64] note that the solution for Φ is inconsistent with CED, which Monstein and Wesley[65] accept as a failure in the classical Maxwell theory. These tests were poorly controlled, and not reproducible.

Butterworth *et al.*[52] unsuccessfully attempted replication of the tests by Monstein and Wesley[51] [TMW], as shown in Table II. The test-to-theory match in Table II refers to the image-charge theory in the previous paragraph. Specifically, both tests placed the antenna at a height $(+H)$ above a large, conductive ground plane. An image-charge model[4] has a negative-charge source at the same distance below the ground plane $(-H)$. However, an image-current flows in the same (opposite) direction as the real current for vertically-(horizontally-) oriented dipole antennas.[46] TMW and the Butterworth[52] omitted the image current, leading to poor agreement between the test results and the models.[66] The last line of Table II refers to measurements of the $\mathbf{E}-$ wave polarization, also as discussed above.

Table III summarizes the inadequacies in these tests and gives suggestions for improvements for the present work. Both experiments have noise that confounds the results. The coaxial feed-line into the antenna creates an asymmetry in the spherical geometry. Lacking a balun, capacitive coupling (displacement current) between the antenna and the coaxial cable's outer conductor induces a return current on the outside of the outer conductor of the coaxial cable, creating TEM radiation (items c-d in Table III). Impedance matching

TABLE II. Comparison of tests by Monstein and Wesley[51] and Butterworth *et al.*[52]

Feature in Monstein and Wesley (2002)	Feature in Butterworth *et al.* (2013)
Aluminum-sphere diameter, $D = 6$ cm	Aluminum-sphere diameter, $D = 7.62$ cm
Antennas on 4.3 m and 4.7 m high stanchions	Antennas on 2 m high stanchions
$f = 433.59$ MHz, $\lambda = 69.2$ cm	$f = 446$ MHz, $\lambda = 67.3$ cm
Signal on and off for calibration purposes	No mention of on/off signal for calibration
Outdoor, north-south test on Rhein River bank	Indoor-hallway/outdoor tests (east-west)
Use of ball antennas only	Ball and half-wave-dipole antennas
No mapping of ball-antenna radiation pattern	Radiation pattern vs angle from ball apex
Transmitter-to-receiver distance, $r = 13 - 700$ m	Transmitter-to-receiver distance, $r = 2 - 90$ m
Test-to-theory match: minima at $r = 24$, 40 m	Test-to-theory match: minimum at $r \sim 30$ m
Longitudinal $\mathbf{E}-$ wave from dipolar polarizer	$\mathbf{E}-$ wave polarization shift by $\pi/2$ radians

TABLE III. Inadequacies in previous experiments and suggested improvements.

Inadequacy in previous experiments	Ways to avoid inadequacies in present work
(a) Frequency too low (433-446 MHz)	Frequency of $\geq$8 GHz for lab test ($\lambda \leq 3.75$ cm)
(b) Poorly controlled, test environment	Use of well-controlled, laboratory environment
(c) Image charge due to conductive grounding	Elimination of return charge by balun
(d) Image current from conductive grounding	Elimination of return current by balun
(e) Imprecise measurements	Use of modern digital instrumentation
(f) Longitudinal polarization from dipole array	Measurement with modern instrumentation
(g) Transmitter-receiver distance error of $\pm$5m	Positional measurements with sub-mm error
(h) No statistical analysis of test-versus-theory	Statistical comparison: experiment with theory

between the source and antenna and signal-to-noise ratio are unaddressed by Monstein and Wesley[51] who used a custom-made transmitter and receiver, instead of a standard signal source and spectrum analyzer. Without a phase-locked signal from a network analyzer, external/stray signals can confound the measurements. The Fresnel zone of the polarizer-analyzer (from diffraction by the circular aperture) is not addressed; the Fresnel radius (F) is ≤ 11 m for the TMW. A small-diameter polarizer-analyzer $(\lambda/F \ll 1)$ does not provide 99% attenuation of the TMW signal in their Fig. 3, unless the polarizer-analyzer is very close to either the transmitter or receiver; that location was unspecified. A definitive test requires better control of the experimental conditions. Thus, these tests do not provide clear SLW evidence.

[1] J. C. Maxwell, Phil. Trans. R. Soc. London **155**, 459 (1865).
[2] O. Heaviside, *Electromagnetic Theory*, Vol. 1 (Cosimo Classics, New York, 2007), Chap. 3, pp. 132ff.
[3] L. Lorenz, Philos. Mag. (Ser. 4) **34**, 287 (1867).
[4] J. D. Jackson, *Classical Electrodynamics* (Wiley, New York, 1962).
[5] J. D. Jackson and L. B. Okun, Rev. Mod. Phys. **73**, 663 (2001).
[6] J. D. Jackson, Am. J. Phys. **70**, 917 (2002).
[7] D. A. Woodside, Am. J. Phys. **77**, 438 (2009).
[8] D. J. Griffiths, *Introduction to Electrodynamics* (Prentice-Hall of India, New Delhi, 2007).
[9] J. A. Stratton, *Electromagnetic Theory* (McGraw-Hill, New York, 1941), p. 5.
[10] A. E. Danese, *Advanced Calculus*, Vol. I (Allyn & Bacon Inc., Boston, MA, 1965).
[11] C. Liu, "Relationship between fields and sources," e-print arXiv:1002.0892v10.
[12] M. Arminjon, Open Phys. **16**, 488 (2018).
[13] B. Jiang, J. Wu, and L. A. Povinelli, J. Comp. Phys. **125**, 104 (1996).
[14] C.-D. Munz, R. Schneider, E. Sonnendrücker, and U. Voss, C. R. Acad. Sci. Paris I **328**, 431 (1999).
[15] C.-D. Munz, P. Omnes, R. Schneider, E. Sonnendrücker, and U. Voß, J. Comp. Phys. **161**, 484 (2000).
[16] M. Pfeiffer, C.-D. Munz, and S. Fasoulas, J. Comp. Phys. **294**, 547 (2015).
[17] E. M. Sousa and U. Shumlak, J. Comp. Phys. **326**, 56 (2016).
[18] L. M. Hively and G. C. Giakos, Int. J. Signal Imaging Syst. Eng. **5**, 3 (2012).
[19] P. Martin-Löf, "Mathematics of infinity," in *COLOG-88* (Lecture Notes in Computer Science), edited by P. Martin-Löf and G. Mints, 417 (Springer, Berlin, 1988).
[20] C. Duval, P. A. Horváthy, and L. Palla, Phys. Rev. D **50**, 6658 (1994).
[21] P. M. Zhang, G. W. Gibbons, and P. A. Horváthy, Phys. Rev. D **85**, 045031 (2012).
[22] G. Rousseaux, R. Kofman, and O. Minazzoli, Eur. Phys. J. D **49**, 249 (2008).
[23] M. Daibo, S. Oshima, Y. Sasaki, and K. Sugiyama, IEEE Trans. Magn. **51**, 1000604 (2015); IEEE Trans. Appl. Supercond. **26**, 0500904 (2016).
[24] R. K. Varma, J. Plasma Phys. **79**, 1025 (2013).
[25] P. K. Shukla, Phys. Scr. **86**, 048201 (2012).
[26] C. G. Camara, J. V. Escobar, J. R. Hird, and S. J. Putterman, Nature (London) **455**, 1089 (2008).
[27] I. Szabò, M. Soddemann, L. Leanza, M. Zoratti, and E. Gulbins, Cell Death Differ. **18**, 427 (2011).
[28] R. G. de Peralta Menendez and S. G. Andino, Comput. Math. Meth. Med. **2015**, 801037.
[29] K. Popper, *Realism and the Aim of Science: From the Postscript to the Logic of Scientific Discovery* (Routledge, London, 1985).
[30] D. A. Woodside, J. Math. Phys. **40**, 4911 (1999).
[31] D. A. Woodside, J. Math. Phys. **41**, 4622 (2000).
[32] F. C. G. Stueckelberg, Helv. Phys. Acta. **11**, 225 (1938); Helv. Phys. Acta. **11**, 299 (1938).
[33] L.-X. Liu and C.-G. Shao, Chin. Phys. Lett. **29**, 111401 (2012).
[34] Y. Aharonov and D. Bohm, Phys. Rev. **130**, 1625 (1963).
[35] J. B. Jiménez and A. L. Maroto, Phys. Rev. D **83**, 023514 (2011).
[36] V. A. Fock and C. Podolsky, *On Quantization of Electro-Magnetic Waves and Interaction of Charges in Dirac Theory* (1932), reprinted in V. A. Fock, *Selected Work—Quantum Mechanics and Quantum Field Theory*, edited by L. D. Faddeev, L. A. Khalfin, and I. V. Komarov (Chapman & Hall/CRC, New York, 2004), pp. 225.
[37] T. Ohmura, Prog. Theor. Phys. **16**, 684 (1956).
[38] K. J. van Vlaenderen and A. Waser, Hadronic J. **24**, 609 (2001).
[39] A. I. Arbab and Z. A. Satti,, Prog. Phys. **5**, 8 (2009).
[40] E. I. Nefyodov and S. M. Smolskiy, *Understanding of Electrodynamics, Radio Wave Propagation and Antennas* (Scientific Research, Wuhan, China, 2012), Chap. 1.
[41] A. K. Tomilin, J. Electromagn. Anal. Appl. **5**, 347 (2013).
[42] A. Gersten and A. Moalem, J. Phys. Conf. Ser. **615**, 012011 (2015).
[43] L. A. Alexeyeva, J. Mod. Phys. **7**, 435 (2016).
[44] G. Modanese, Results Phys. 7, 480 (2017); Mod. Phys. Lett. B 31, 1750052 (2017); Phys. B 524, 81 (2017); Mathematics **6**, 155 (2018); *Tunneling*, *Unified Field Mechanics II: Formulations and Empirical Tests* (World Scientific, Hackensack, NJ, 2018), pp. 268ff.
[45] M. Planck, Sitz. d. Königlich Preußischen Akad. Wiss. Berlin **5**, 440 (1899).
[46] P. Lorrain and D. R. Corson, *Electromagnetic Fields and Waves*, 2nd ed. (W.H. Freeman and Co., San Francisco, CA, 1970).
[47] L. B. Okun, Sov. Phys. Usp. **32**, 543 (1989).
[48] M. Agostini, S. Appel, G. Bellini, J. Benziger, D. Bick, G. Bonfini, D. Bravo, B. Caccianiga, F. Calaprice, A. Caminata, P. Cavalcante, A. Chepurnov, D. D'Angelo, S. Davini, A. Derbin, L. D. Noto, I. Drachnev, A. Empl, A. Etenko, K. Fomenko, D. Franco, F. Gabriele, C. Galbiati, C. Ghiano, M. Giammarchi, M. Goeger-Neff, A. Goretti, M. Gromov, C. Hagner, E. Hungerford, A. Ianni, A. Ianni, K. Jedrzejczak, M. Kaiser, V. Kobychev, D. Korablev, G. Korga, D. Kryn, M. Laubenstein, B. Lehnert, E. Litvinovich, F. Lombardi, P. Lombardi, L. Ludhova, G. Lukyanchenko, I. Machulin, S. Manecki, W. Maneschg, S. Marcocci, E. Meroni, M. Meyer, L. Miramonti, M. Misiaszek, M. Montuschi, P. Mosteiro, V. Muratova, B. Neumair, L. Oberauer, M. Obolensky, F. Ortica, K. Otis, M. Pallavicini, L. Papp, L. Perasso, A. Pocar, G. Ranucci, A. Razeto, A. Re, A. Romani, R. Roncin, N. Rossi, S. Schönert, D. Semenov, H. Simgen, M. Skorokhvatov, O. Smirnov, A. Sotnikov, S. Sukhotin, Y. Suvorov, R. Tartaglia, G. Testera, J. Thurn, M. Toropova, E. Unzhakov, A. Vishneva, R. B. Vogelaar, F. von Feilitzsch, H. Wang, S. Weinz, J. Winter, M. Wojcik, M. Wurm, Z. Yokley, O. Zaimidoroga, S. Zavatarelli, K. Zuber, and G. Zuzel, Phys. Rev. Lett. **115**, 231802 (2015).

[49]A. Jedele, A. B. McIntosh, K. Hagel, M. Huang, L. Heilborn, Z. Kohley, L. W. May, E. McCleskey, M. Youngs, A. Zarrella, and S. J. Yennello, Phys. Rev. Lett. **118**, 062501 (2017).
[50]S. Jezouin, Z. Iftikhar, A. Anthore, F. D. Parmentier, U. Gennser, A. Cavanna, A. Ouerghi, I. P. Levkivskyi, E. Idrisov, E. V. Sukhorukov, L. I. Glazman, and F. Pierre, Nature (London) **536**, 58 (2016).
[51]C. Monstein and J. P. Wesley, Europhys. Lett. **59**, 514 (2002).
[52]F. J. Butterworth, C. B. Allison, D. Cavazos, and F. M. Mullen, J. Sci. Explor. **27**, 13 (2013).
[53]P. W. Graham, J. Mardon, S. Rajendran, and Y. Zhao, Phys. Rev. D **90**, 075017 (2014).
[54]S. Ramo, J. R. Whinnery, and T. van Duzer, *Fields and Waves in Communication Electronics* (John Wiley & Sons, New York, 1967), pp. 332ff.
[55]S. Axler, P. Bourdon, and W. Ramey, *Harmonic Function Theory* (Springer, New York, 2001).
[56]A. D. Polyanin, *Handbook of Linear Partial Differential Equations for Engineers and Scientists* (Chapman & Hall/CRC, Boca Raton, FL, 2001).
[57]P. Swallow, "Practical VHF/UHF antennas," in *The Radio Communication Handbook*, 12th ed. (The Radio Society of Great Britain, London, 2008), Chap. 16.
[58]T. Nakatani, J. Rode, D. F. Kimball, L. F. Larson, and P. M. Asbeck, IEEE J. Solid-State Circ. **47**, 1104 (2012).
[59]C. Capps, Electrical Design News (16 August 2001). pp. 95.
[60]W. K. H. Panofsky and M. Phillips, *Classical Electricity and Magnetism*, 2nd ed. (Addison-Wesley, Reading, MA, 1962), pp. 270.
[61]J. Earman and D. Fraser, Erkenntnis **64**, 305 (2006).
[62]E. Seidewitz, Found. Phys. **47**, 355 (2017).
[63]C. Itzykson and J. Zuber, *Quantum Field Theory* (McGraw-Hill, New York, 1980).
[64]J. R. Bray and M. C. Britton, Europhys. Lett. **66**, 153 (2004).
[65]C. Monstein and J. P. Wesley, Europhys. Lett. **66**, 155 (2004).
[66]K. Rebilas, Europhys. Lett. **83**, 60007 (2008).